Role of electronic correlations in the kagome-lattice superconductor LaRh$_3$B$_2$

Savita Chaudhary [1] Shama,[1] Jaskaran Singh,[1,2] Armando Consiglio,[3] Domenico Di Sante,[4,5]
Ronny Thomale,[3] and Yogesh Singh [1]

[1]*Department of Physical Sciences, Indian Institute of Science Education and Research (IISER) Mohali,*
Knowledge City, Sector 81, Mohali 140306, India
[2]*Department of Physics, Punjabi University, Patiala 147002, India*
[3]*Institut für Theoretische Physik und Astrophysik and Würzburg-Dresden Cluster of Excellence ct.qmat,*
Universität Würzburg, 97074 Würzburg, Germany
[4]*Department of Physics and Astronomy, Alma Mater Studiorum, University of Bologna, 40127 Bologna, Italy*
[5]*Center for Computational Quantum Physics, Flatiron Institute, 162 5th Avenue, New York, New York 10010, USA*

LaRh$_3$B$_2$ crystallizes in a layered structure where Rh atoms form a perfect kagome lattice. The material shows superconductivity at $T_c \approx 2.6$ K and no signature for density wave instabilities. We report our measurements of electronic transport, magnetization, and heat capacity in the normal and superconducting state, and we derive normal and superconducting parameters. From first-principles calculations of the electronic band structure, we identify all features of kagome bands predominantly formed by the Rh d orbitals: a flat band, Dirac cones, and van Hove singularities. The calculation of the phonon dispersions and electron-phonon coupling suggests a strong similarity between LaRh$_3$B$_2$ and AV$_3$Sb$_5$ (A = K,Cs,Rb). For LaRh$_3$B$_2$, it matches quantitatively with the observed T_c, supporting a conventional phonon-mediated pairing mechanism. By comparison to the AV$_3$Sb$_5$ family, we conjecture that there is a reduced importance of electron correlations in LaRh$_3$B$_2$.

I. INTRODUCTION

The kagome lattice has long been a playground for novel physics in condensed matter. Insulating kagome-lattice realizations with localized magnetic moments are platforms to explore the effects of geometric magnetic frustration. The quantum spin liquid (QSL) ground state in the mineral herbertsmithite ZnCu$_3$(OH)Cl$_2$ is a prime example of this behavior [1,2]. Insulating quantum magnets with a kagome network in higher dimensions have also shown novel frustrated magnetism and QSL behavior [3–5]. More recently, metallic kagome lattice materials have been brought into focus due to the prediction that the electronic structure of electrons on a kagome lattice might allow us to access correlated Dirac cones or van Hove singularities near the Fermi energy [6–8]. The two-dimensional kagome lattice has features in its band structure that provide, even still in the itinerant limit, the opportunity to marry nontrivial topology and strong electron correlations. The search for realizations of a material with an ideal isolated kagome lattice is therefore a fundamentally important quest. In recent years, a few families of metallic materials possessing a kagome lattice have indeed been reported or theoretically predicted. These include the herbertsmithite-related material Ga/ScCu$_3$(OH)$_6$Cl$_2$ [8], the magnetic kagome metals CoSn and FeSn [9,10], and the ferromagnetic kagome metal YMn$_6$Sn$_6$ [11]. Most recently, the AV$_3$Sb$_5$ (A = K, Rb, Cs) family of materials have been discovered and shown to host a perfect kagome network of V ions [12,13]. Evidence for electron correlations and

nontrivial topology in these materials emerges from the discovery of charge density waves, superconductivity, the anomalous Hall effect, and multiple van Hove singularities near the Fermi energy [12,14–16].

Another family of materials possessing the kagome lattice is RT_3X_2 (R = lanthanide, T = 4d or 5d transition metal, X = Si,B). These materials were discovered in the 1980s [17–19], and several of them were reported to show superconductivity with T_c between 1 and $\sim$7 K [17–22]. However, most of these studies were not carried out in the context of the connection of properties with the underlying kagome lattice. It was only recently that LaRu$_3$Si$_2$, which has the highest $T_c = 7$ K in this family of materials, and YRu$_3$Si$_2$ were studied in relation to the kagome lattice, and several unconventional properties have been reported, possibly arising from electron correlations from the flat bands [23–27]. Materials in the RT_3X_2 family thus form another promising platform to study the kagome-related features in the band structure, and their interplay with superconductivity.

We report on the electronic structure, phonon profile, and superconducting properties of LaRh$_3$B$_2$, which has previously been reported to show superconductivity at low temperatures, where the reported superconducting T_c ranges from <1.2 to 2.8 K [17,20]. Our electronic band-structure calculations reveal a flat band above the Fermi energy, and van Hove singularities and Dirac cones at several locations in the Brillouin zone including close to the Fermi energy E_F. We find that the E_F is located at the top of a sharp peak in the density of states (DOS). We use this to address the extreme sample dependence

of the superconducting T_c. The superconductivity is found to be of conventional weak-coupling type. This is supported by estimations of the T_c from phonon calculations and the estimate of electron-phonon coupling. The van Hove singularities in the band structure are found to be located a few eV away from E_F, which is large against the characteristic ordering scales and thus explains why these materials do not show signals of correlation-induced phenomena such as charge-density waves or other instabilities. This is also supported by the phonon calculations, which stress the absence of any imaginary frequency mode. In addition, we observe anomalous temperature dependencies of the magnetic susceptibility and heat capacity, and a slightly enhanced Sommerfeld coefficient, which we argue arises from the narrow band which is part of the DOS. In comparison with the AV_3Sb_5 materials, our results point to a reduced importance of electronic correlations in the $LaRh_3B_2$ material.

II. METHODS

Polycrystalline samples of $LaRh_3B_2$ were synthesized by arc-melting stoichiometric ratios of La (3N, Alfa Aesar), Rh (5N, Alfa Aesar), and B (6N, Alfa Aesar). The melted buttons were flipped over and melted 5–10 times to promote homogeneity. Powder x-ray diffraction (PXRD) on a Bruker D8 Advance diffractometer system with Cu $K\alpha$ radiation was used to determine the phase purity of the arc-melted $LaRh_3B_2$ sample. The relative stoichiometry of La and Rh was confirmed using energy-dispersive spectroscopy using a scanning electron microscope. The dc magnetic susceptibility χ, heat capacity C, and electrical transport were measured using a Quantum Design Physical Property Measurement System equipped with an He3 insert. To theoretically simulate the electronic structure of $LaRh_3B_2$, we performed first-principles density functional theory (DFT) calculations using the Vienna Ab initio simulation package (VASP) [28–31]. We considered the projector-augmented wave (PAW) pseudopotential with exchange-correlation functional of the generalized gradient approximation (GGA) of Perdew-Burke-Ernzerhof [32,33]. Starting with the experimental structure, the lattice relaxation was performed to optimize the crystal structure by using variable cell relaxation. We adopted a $12 \times 12 \times 12$ k mesh for the first Brillouin zone. We have used an energy cutoff of 450 eV for the plane-wave basis. The convergence criteria for energy and force are set to 10^{-6} eV and 0.02 eV/Å, respectively. In the DFT calculation, spin-orbit coupling was not included. However, we have used a scalar relativistic potential, which takes scalar relativistic effects into account. Phonon calculations have been performed using density functional perturbation theory, as implemented in QUANTUM ESPRESSO [34–36]. Exchange and correlation effects were included using the generalized gradient approximation (GGA) with the Perdew-Burke-Ernzerhof (PBE) functional [33]; the pseudopotentials are norm-conserving, with core correction, and scalar relativistic [37].

Self-consistent calculations of the previously relaxed unit cell have been performed with an $8 \times 8 \times 12$ k-grid. The kinetic energy cutoff for the wave functions is equal to 100 Ry, while the cutoff for charge density is 400 Ry. Convergence threshold for ionic minimization and electronic
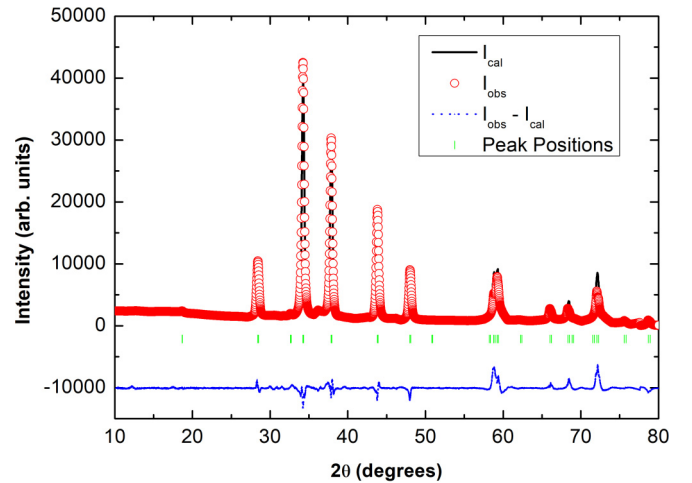

FIG. 1. Powder x-ray diffraction and results of refinement.

self-consistency are set to be 1.0D-15. The self-consistency threshold for phonon calculations is 1.0D-15 as well, with a q-grid of $4 \times 4 \times 2$. Non-self-consistent calculations for the density of states have been performed with a $60 \times 60 \times 48$ k-grid. Finally, the electron-phonon interaction is computed via an interpolation over the Brillouin zone [38].

III. STRUCTURE

$LaRh_3B_2$ crystallizes in a honeycomb structure with space group $P6/mmm$. There are no variable parameters in the structure apart from the unit cell size. The powder x-ray diffraction (PXRD) is shown in Fig. 1. The PXRD pattern confirmed that the synthesized material is single-phase, and a refinement, shown in Fig. 1, of the powder pattern gave lattice parameters $a = 5.486$ Å and $c = 3.136$ Å. A range of values for the lattice parameters has been reported in the literature, and our values fall within that range [17]. We will make a connection of unit cell parameters with the electronic properties later. A schematic of the crystal structure of $LaRh_3B_2$ is shown in Fig. 2. The structure is made up of layers of Rh planes separated by planes of La and B stacked along the c-axis, as shown in Fig. 2(a). The arrangement of the Rh atoms within the Rh planes is a perfect kagome lattice, as shown in Fig. 2(b). These materials, therefore, have the structural ingredients to show electronic structure features expected for a kagome metal. It must be noted however, that the short c-axis necessarily means that coupling between kagome planes may be significant.

IV. RESULTS

A. Electronic band structure

Figure 3(a) shows the electronic band structure for $LaRh_3B_2$ along some high-symmetry directions in the Brillouin zone. It is evident that several bands cross the Fermi level, confirming that $LaRh_3B_2$ is a metal. The total and partial density of states (DOS) are shown in Fig. 3(b). The Fermi level (E_F) is situated near the top of a very narrow band resulting in a fairly large DOS at E_F of 6.6 states/eV. From the partial DOS it is clear that the majority contribution to the total
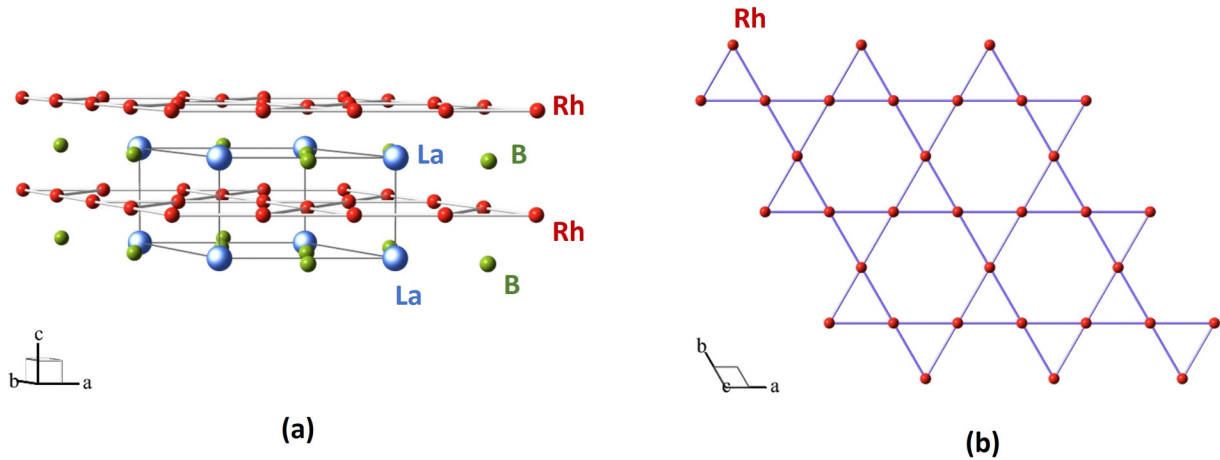
FIG. 2. (a) A schematic of the crystal structure of $LaRh_3B_2$ viewed perpendicular to the crystallographic c-axis showing the layered nature of the structure with Rh atomic planes separated along the c-axis by planes made up of La and B atoms. (b) Viewed along the c-axis, the Rh atoms form an undistorted kagome lattice.

DOS comes from Rh $4d$ orbitals, and both La and B contribute very small amounts to the total DOS at E_F. The narrow band at E_F leads to a strong sensitivity of the superconducting T_c on the unit cell size and to other anomalous physical properties, as we will discuss later.

We now turn to the novel features of the band structure arising from the kagome Rh planes. As can be seen in Fig. 3(a), we observe a flat band (FB) in the Γ-M-K-Γ direction about 0.4 eV above E_F. This flat band is separate from any other bands. Another series of disconnected flat bands is observed along the Γ-A direction about 0.75 eV above E_F. In addition to these flat portions of the electronic dispersion, Dirac cones (DCs) are observed at several locations in the band structure. There are Dirac bands 140 meV below and 2.75 eV above E_F at H and a Dirac cone about 1 eV below E_F along the M-K direction in the BZ. We also identify van Hove (VH) singularities located symmetrically above and below the Dirac cone at 2.75 eV. Thus the band structure of $LaRh_3B_2$ possesses the predicted features of the kagome-lattice band structure

near E_F with modifications arising most likely from the three-dimensional nature of the material.

B. Physical properties

Figure 4 shows the electrical, magnetic, and thermal properties of $LaRh_3B_2$ in the normal and superconducting states. Figure 4(a) shows the magnetic susceptibility χ versus temperature T between 2 and 300 K in an applied magnetic field of $H = 2$ T. At low temperatures, small amounts of magnetic impurities lead to a Curie-like upturn. The χ is found to be temperature-dependent in the whole temperature range. This is not what is expected for a Pauli paramagnetic metal where a T-independent χ is expected. This T-dependent χ arises due to the E_F being situated on a narrow peak in the DOS. The change in temperature results in a change in the DOS at E_F leading to a T-dependent Pauli paramagnetic susceptibility. To support this idea, the $\chi(T)$ in the full temperature range was fit with the expression
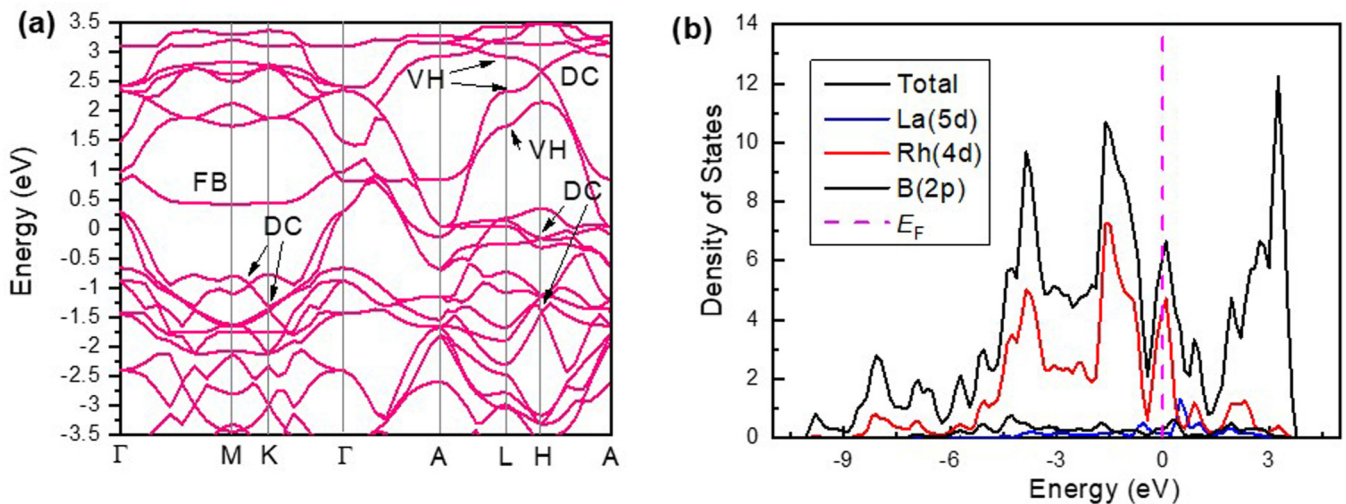

FIG. 3. (a) The electronic structure of $LaRh_3B_2$ along high-symmetry directions in k-space. The boxes are to highlight some interesting features as discussed in the main text. (b) The total and partial density of states as a function of energy measured from the Fermi energy.
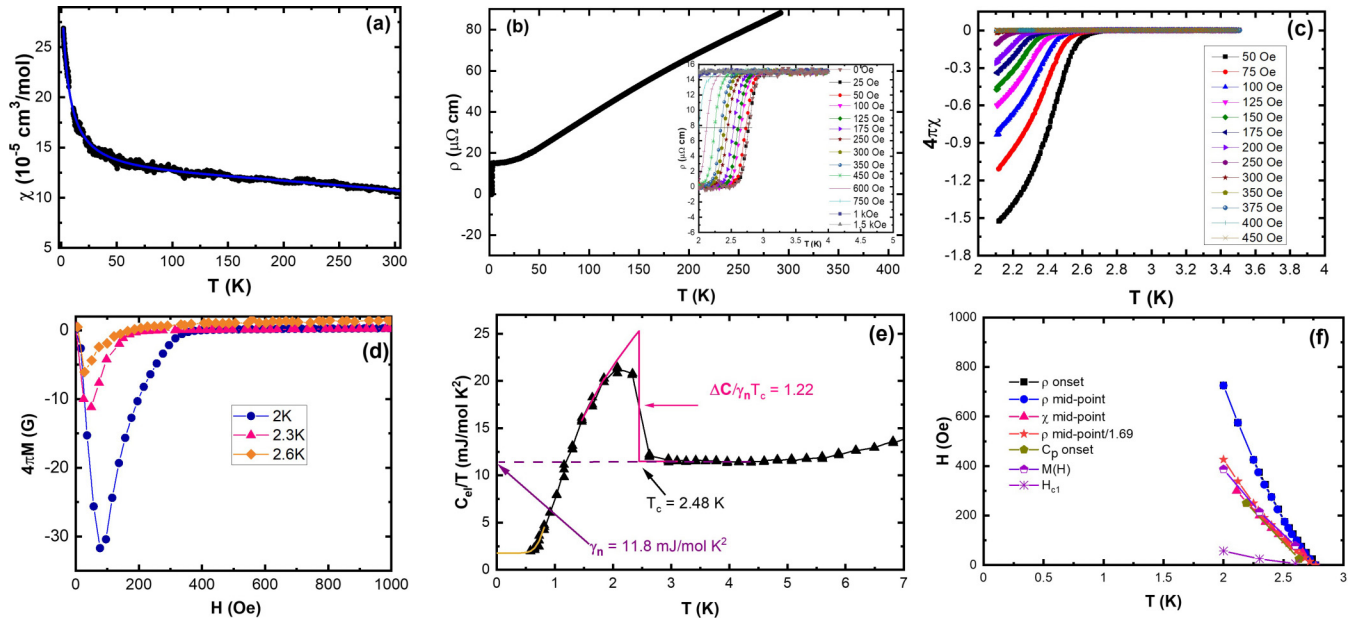
FIG. 4. (a) The normal-state magnetic susceptibility at $H = 2$ T, and (b) resistivity vs temperature at zero field. The inset shows the superconducting transition at various fields, (c) dimensionless magnetic susceptibility ($4\pi\chi$) in the superconducting state at various fields, and (d) the electronic contribution to the zero-field specific heat C_{el}/T vs T.

$\chi(T) = \chi_o[1 - (T/T_E)^2] + C/(T - \theta)$, where the first term represents the T-dependent Pauli paramagnetic susceptibility, and the second term represents the contribution from the small amounts of magnetic impurities that give rise to the Curie-like upturn in $\chi(T)$ at the lowest temperatures. The fitting parameters are χ_o, which is the temperature-independent average Pauli paramagnetic susceptibility; T_E, which is a phenomenological parameter related to the Fermi energy; C, which is the Curie constant of the impurities; and θ, which is the Weiss temperature representing any interactions between the magnetic impurities. A very good fit with the above expression was obtained and is shown as the solid curve through the data in Fig. 4(a). The fit parameters obtained were $\chi_o = 11.8(2) \times 10^{-5}$ G cm^3/mol, $T_E = 860(7)$ K, $C = 0.0010(4)$ G cm^3 K/mol, and $\theta = -5.5(1)$ K. This value of C is equivalent to 0.25% of $S = 1/2$ impurities, which is quite small.

Figure 4(b) shows the electrical resistivity ρ in zero field between 2 and 300 K. We observe metallic behavior with a residual resistivity ratio RRR = $\rho(300$ K$)/\rho(2$ K$) \approx 5$. The inset in Fig. 4(b) shows the $\rho(T)$ data below $T = 4$ K measured in various applied fields. The sharp drop to zero resistance below $T_c \sim 2.6$ K in zero field signals the onset of superconductivity in LaRh$_3$B$_2$. Further evidence of a superconducting state is obtained from the diamagnetism observed in magnetic measurements shown in Figs. 4(c) and 4(d). From Fig. 4(c) we can see that the value of $4\pi\chi$ in the superconducting state is greater than -1, suggesting demagnetization factors due to the irregular shape of the sample. The magnetization data in Fig. 4(d) show behavior typical of a type-II superconductor with a small Ginzburg-Landau parameter κ. The bulk nature of superconductivity is confirmed from heat-capacity measurements. Figure 4(e) shows the electronic heat capacity C_{el} divided by T versus T. The C_{el} is obtained by subtracting a lattice term ($\sim T^3$) from the total heat capacity. It is of interest to note that the C_{el}/T in the normal state

would be expected to be T-independent. However, this is true only for $T \leqslant 4.5$ K, while there is a strong T dependence of C_{el}/T above these temperatures. This suggests that the lattice contribution may not just have a T^3 term, but anharmonic terms may also contribute to the lattice heat capacity. A sharp anomaly at the onset of the superconducting transition can clearly be seen in Fig. 4(e). To evaluate the magnitude of the jump in heat capacity at the transition and to obtain an alternate estimate of the bulk superconducting T_c, we use an equal entropy construction. The result is shown as the solid curve through the data near T_c. This gives a value $T_c \approx 2.5$ K. The normal state data above T_c can be extrapolated to $T = 0$ to give an estimate of the Sommerfeld coefficient $\gamma_n = 11.8$ mJ/mol K^2. With this we obtain the jump height at T_c to be $\Delta C_{el}/\gamma_n T_c \approx 1.2$, which is smaller than the value 1.43 expected for a weak-coupling single-gap superconductor. The C_{el} data at the lowest temperatures seem to extrapolate to a finite value suggesting some residual contribution from normal electrons. The C_{el} data below $T = 0.8$ K were fit by the expression $C_{el} = \gamma_{res} T + A \exp^{-\Delta/k_B T}$ assuming a fully gapped superconducting state. The $\gamma_{res} T$ term represents the contribution from any nonsuperconducting fraction of electrons. An excellent fit, shown in Fig. 4(e), was obtained with the following values for the parameters: $\gamma_{res} = 1.7$ mJ/mol K^2 and $\Delta = 6$ K. This value of γ_{res} suggests that $\approx 14\%$ electrons do not participate in the superconductivity. So we must revise our estimate of $\Delta C_{el}/\gamma T_c$ using $\gamma = \gamma_n - \gamma_{res}$. This gives the value $\Delta C_{el}/\gamma T_c \approx 1.44$, which is close to the value expected from a weak-coupling single gap superconductor. These results suggest that LaRh$_3$B$_2$ is a weak-coupling single-gap type-II superconductor.

From various measurements in finite magnetic field, we can track the T_c as a function of the field H. The H-T diagram obtained from the various measurements is shown in Fig. 4(f), where both the lower critical field H_{C1} and the upper critical

field H_{C2} are shown. We observe that the H_{C2} data from all measurements except the resistivity measurements agree with each other, while the critical field measured from ρ is consistently higher than the values measured from other bulk probes like magnetization and heat capacity. Such observations have been reported previously in some materials and have been linked to surface superconductivity [39,40]. It has been shown that the critical field for surface superconductivity is $\approx 1.69 H_{c2}$, where H_{c2} is the bulk critical field. We also plot in Fig. 4(f) the H_{C2} obtained from resistivity measurements divided by 1.69. The critical field so obtained matches the critical field values obtained from other bulk measurements. So we will treat the scaled critical field from resistivity measurements as the true bulk critical field H_{c2}. The H_{c2} versus T plot shows an upward curvature in the whole temperature range. This is unusual and inconsistent with observations for most conventional superconductors. An upward curvature has been previously reported for some families of unconventional superconductors such as the cuprates, superconducting spin-ladders, and organics [41,42], and also for multigap superconductors such as MgB_2 [43] or $OsB2$ [44]. We also find in the literature reports of observations of an upward curvature near T_c in H_{c2}-T plots for superconductors which have some disorder, such as hydrated Na_xCoO_2 [45,46] and NbN [47]. The material $LaRh_3B_2$ seems to be a conventional and single-band superconductor. We will also show later that the transport properties and indeed T_c are sample-dependent. So while it is not clear why we observe this upward curvature in the H_{c2}-T plots, disorder may play a role.

To learn about the strength of the electron-phonon coupling, we make an estimate of the electron-phonon coupling constant λ_{ep} using McMillan's formula, which relates the superconducting transition temperature T_c to λ_{ep}, the Debye temperature θ_D, and the Coulomb repulsion constant μ^*,

$$T_c = \frac{\Theta_D}{1.45} \exp\left[-\frac{1.04(1 + \lambda_{ep})}{\lambda_{ep} - \mu^*(1 + 0.62\lambda_{ep})}\right],$$

which can be inverted to give λ_{ep} in terms of T_c, θ_D, and μ^* as

$$\lambda_{ep} = \frac{1.04 + \mu^* \ln\left(\frac{\Theta_D}{1.45 T_c}\right)}{(1 - 0.62\mu^*) \ln\left(\frac{\Theta_D}{1.45 T_c}\right) - 1.04}.$$

From the heat-capacity measurements we had obtained $\theta_D = 518$ K, and using $T_c = 2.5$ K we get $\lambda_{ep} = 0.43$ and 0.56 for $\mu^* = 0.10$ and 0.17, respectively. These values of λ_{ep} suggest moderate electron-phonon coupling in $LaRh_3B_2$. This is supported by the estimates of the λ_{ep} made from our phonon calculations, which will be discussed later.

We now present our estimation of various superconducting parameters using expressions previously collected in Refs. [44,48]. An estimate of the $T = 0$ upper critical field $H_{c2}(0)$ was made by first making a linear extrapolation of the data near T_c to give the slope $\frac{dH_{c2}}{dT}\big|_{T_c} = -511$ Oe/K. This linear slope can then be used to get an estimate of $H_{c2}(0)$ using the Werthamer-Helfand-Hohenberg (WHH) formula for the clean limit $H_{c2}(0) = -0.693 T_c \frac{dH_{c2}}{dT}\big|_{T_c} = 920$ Oe. From the value of H_{c2} we can now estimate the value of the coherence length ξ by the expression $H_{c2} = \phi_0/2\pi\xi^2$, where $\phi_0 = hc/2e = 2.068 \times 10^{-7}$ G cm^2 is the flux quantum.

TABLE I. Normal and superconducting state parameters for $LaRh_3B_2$. Here γ is the Sommerfeld coefficient, β is the coefficient of the T^3 term in the low-temperature heat capacity, θ_D is the Debye temperature, n is the electron density, ξ is the superconducting coherence length, λ is the penetration depth, l is the electron mean free path, and v_F is the Fermi velocity.

RRR	≈ 5
γ (mJ/mol K^2)	11.8
β (mJ/mol K^4)	0.084
θ_D (K)	520
n (cm^{-3})	1.2×10^{23}
T_C (K)	2.6
ξ_{2K} (nm)	114
ξ_{0K} (nm)	60
λ_{0K} (nm)	59.4
κ_{0K}	0.9
l_{4K} (nm)	43
v_F (cm/s)	1.7×10^8

Using $H_{c2}(0) = 920$ Oe obtained above, we estimate $\xi(0) = 60$ nm. At $T = 2.3$ K near T_c, where $H_{c2} = 250$ Oe, we get $\xi(0) = 114$ nm. We have collected the various normal and superconducting state parameters in Table I.

We now address the large variation in the T_c of $LaRh_3B_2$, which has been reported in the literature [17,20]. Figure 5 shows the resistivity of two samples of $LaRh_3B_2$ prepared with the same nominal ratios of starting materials. A refinement of their powder x-ray pattern gave lattice parameters that are slightly different. The lattice parameters for sample 1 (S1) are $a = 5.484$ Å and $c = 3.139$ Å while those for sample 2 (S2) are $a = 5.486$ Å and $c = 3.136$ Å. Thus the S1 has slightly smaller in-plane lattice parameters while its c-axis is longer indicating that in this sample the kagome planes are shrunk while the separation between the kagome lattice increases. S2, on the other hand, has a larger kagome plane
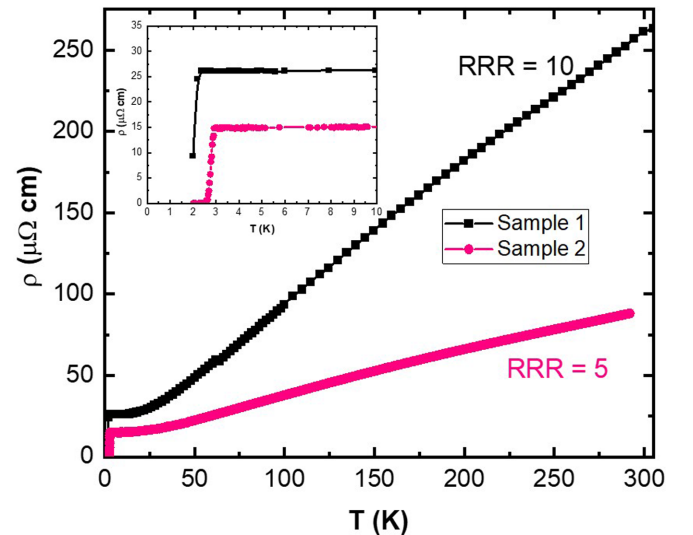

FIG. 5. Resistivity vs temperature at zero field for two $LaRh_3B_2$ samples. The inset shows the variation in the superconducting transition temperature.
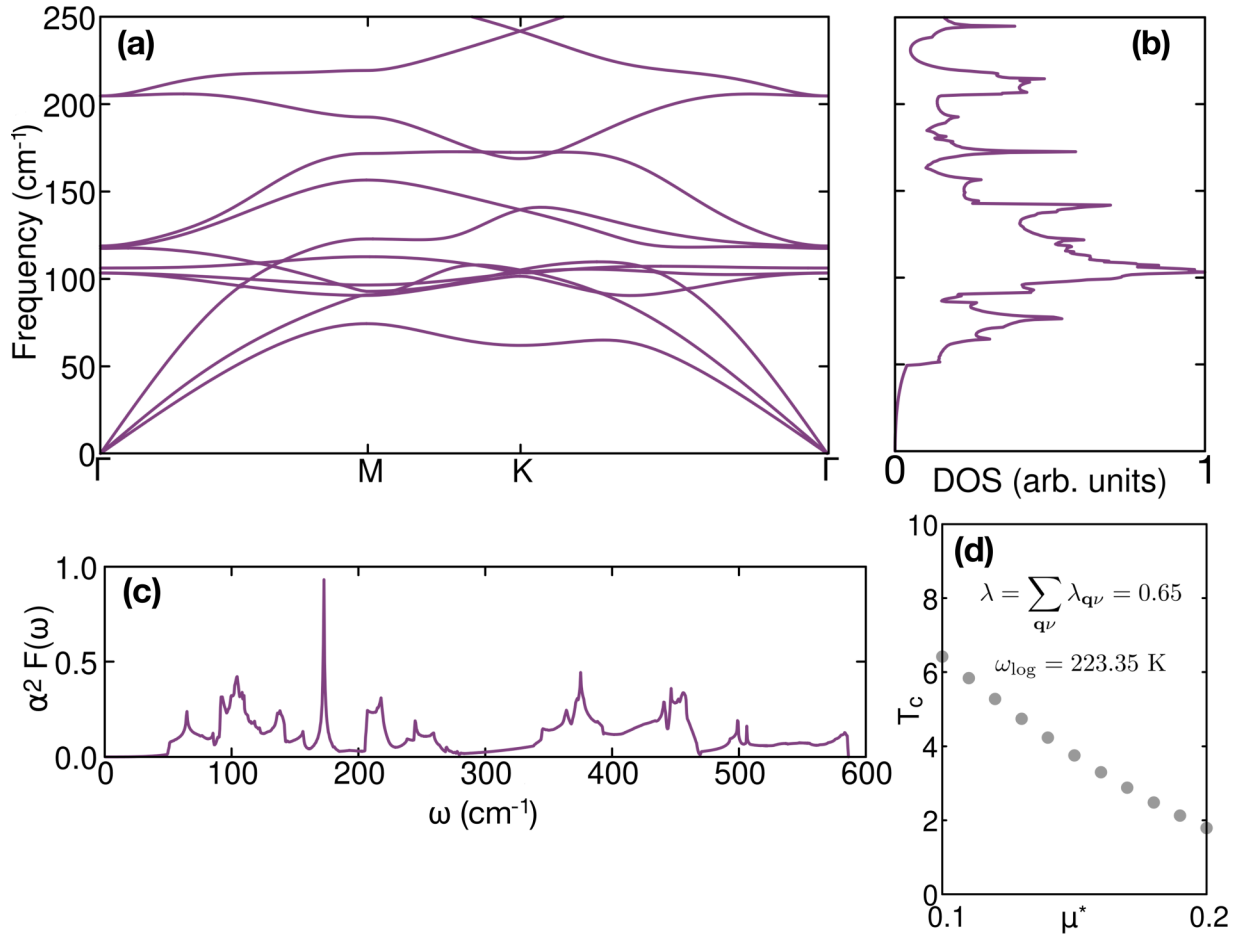
FIG. 6. (a) Phonon dispersion along high-symmetry lines; (b) corresponding density of states; (c) Eliashberg spectral function as a function of phonon frequency ω. Note the following conversion factors: $1\,\text{THz} = 4.136\,\text{meV} = 33.356\,\text{cm}^{-1}$. (d) Superconducting critical temperature T_c (K) as a function of the Coulomb pseudopotential μ^*.

but the planes are separated by a smaller distance along the c-axis. From Fig. 5 we see that the electrical transport properties are sensitive to these small changes. S1 has a larger residual resistivity ratio RRR $= 10$ but has a larger residual resistivity $\rho_0 = 26\,\mu\Omega\,\text{cm}$. S2, on the other hand, has a smaller RRR $= 5$ but a smaller residual resistivity $\rho_0 = 15\,\mu\Omega\,\text{cm}$. From the inset it can be seen that while S2 has a superconductivity onset at $T_c = 2.6$ K, for S1 the onset is $T_c = 2.05$ K, more than 0.5 K lower. We also find this large variation in T_c with unit cell size of LaRh$_3$B$_2$ in previous reports [17,20]. For example, superconductivity with $T_c = 2.6$ K was reported for a LaRh$_3$B$_2$ sample with lattice parameters $a = 5.480$ Å and $c = 3.137$ Å [17], $T_c = 2.2$ K was reported for a sample with lattice parameters $a = 5.483$ Å, $c = 3.142$ Å, while no superconductivity down to 1.2 K was found for a sample with lattice parameters $a = 5.512$ Å and $c = 3.115$ Å [20].

We can address this variation in T_c for different samples using our DFT calculations. Our calculations have shown that the E_F lies near the top of a narrow band in the DOS. This sensitivity of T_c most likely originates from changes in the DOS at E_F due to small changes in E_F either by pressure effects (as evidenced by the difference in unit cell sizes) or due to a difference in the electron densities (by minute

variation in the stoichiometry) in the samples. A slight change in E_F will lead to large changes in the DOS at E_F because the E_F is located on top of a narrow band in the band structure.

Our phonon calculations support the motif of weak-coupling phonon-mediated superconductivity, and they also indicate the reason for the absence of a correlation-induced CDW instability for LaRh$_3$B$_2$. The phonon dispersion for LaRh$_3$B$_2$ is shown in Figs. 6(a) and 6(b). The phonon dispersion does not exhibit any imaginary frequency mode; this is a sign of dynamical stability, confirming the absence of experimental signatures of charge-density-wave states. Low-frequency phonon modes mostly originate from La atoms, while intermediate frequencies are essentially due to Rh atoms; the manifold of low-dispersing bands around 120 cm^{-1} is then due to the kagome network. Finally, B atoms contribute to the high-frequency modes. We computed the electron-phonon coupling to be $\lambda_{\text{ep}} \approx 0.55$–$0.65$. This suggests that LaRh$_3$B$_2$ is a weak- to moderate-coupling superconductor. The McMillan formula was then used to estimate the superconducting critical temperature T_c [49,50]:

$$T_c = \frac{\omega_{\text{log}}}{1.2} e^{\left[\frac{-1.04(1+\lambda_{\text{ep}})}{\lambda_{\text{ep}}(1-0.62\mu^*)-\mu^*}\right]} \quad (1)$$

with $\omega_{\log}$ being related to the Eliashberg function:

$$\omega_{\log} = e^{\left[\frac{2}{\lambda_{\text{ep}}} \int \frac{d\omega}{\omega} \alpha^2 F(\omega) \log \omega\right]}. \tag{2}$$

While the Coulomb pseudopotential μ^* lies in the typical range [0.1–0.2], we obtain values for T_c in fair agreement with the experimental results. Specifically, $T_c \approx 2.6$ K is obtained for $\mu^* = 0.17$ [Fig. 6(d)].

V. SUMMARY AND DISCUSSION

We report on the electronic structure, phonon spectrum, and physical properties of a kagome-lattice superconductor $LaRh_3B_2$. The structure of $LaRh_3B_2$ is made up of kagome planes of Rh stacked along the c-axis with La-B planes separating the kagome planes. The electronic structure contains all features expected for a 2D kagome lattice including a flat band and Dirac bands and van Hove singularities at various positions in the Brillouin zone and in particular near E_F. This is qualitatively consistent with the band structure observed for the AV_3Sb_5 kagome metals. In contrast with the AV_3Sb_5 materials, however, we did not observe signatures of strong electronic correlations in $LaRh_3B_2$. The van Hove singularities in the electronic band structure are situated farther away from E_F than for AV_3Sb_5, which is a fermiological reason why one would not expect charge ordering or density-wave-like instabilities as reported for AV_3Sb_5.

The superconductivity in $LaRh_3B_2$ seems conventional, and there is no experimental evidence for charge-density-wave instabilities as reported for the AV_3Sb_5 materials. The majority contribution to the DOS at E_F in $LaRh_3B_2$ derives from Rh $4d$ bands. This suggests that the role of electronic correlations is weakened in $LaRh_3B_2$ compared to the family of AV_3Sb_5 kagome metals, since the Rh $4d$ orbitals are less strongly correlated than the V $3d$ orbitals. Interestingly, the computed λ_{ep} for $LaRh_3B_2$ is in good agreement with experimentally reported values of λ_{ep} for the CsV_3Sb_5 compound [51], which, together with the phonon dispersions, suggests a similarity in the principal phonon sector between $LaRh_3B_2$ and AV_3Sb_5. It suggests that a central difference between $LaRh_3B_2$ and the by now more established kagome metals must be found in terms of differing electronic correlations, which are lower in strength for $LaRh_3B_2$. This may explain the absence of CDW in the $LaRh_3B_2$ kagome metal, and it points towards phonon-mediated s-wave superconductivity. Given the large number of materials in the RT_3B_2 and RT_3Si_2 families, their possibility of fermiology-tuning around E_F presents an exciting direction for future work.

[1] M. Fu, T. Imai, T.-H. Han, and Y. S. Lee, Science **350**, 655 (2015).

[2] T.-H. Han, J. S. Helton, S. Chu, D. G. Nocera, J. A. Rodriguez-Rivera, C. Broholm, and Y. S. Lee, Nature (London) **492**, 406 (2012).

[3] C. Balz, B. Lake, J. Reuther, H. Luetkens, R. Schönemann, T. Herrmannsdörfer, Y. Singh, A. T. M. Nazmul Islam, E. M. Wheeler, J. A. Rodriguez-Rivera, T. Guidi, G. G. Simeoni, C. Baines, and H. Ryll, Nat. Phys. **12**, 942 (2016).

[4] Y. Okamoto, M. Nohara, H. Aruga-Katori, and H. Takagi, Phys. Rev. Lett. **99**, 137207 (2007).

[5] Y. Singh, Y. Tokiwa, J. Dong, and P. Gegenwart, Phys. Rev. B **88**, 220413(R) (2013).

[6] M. L. Kiesel, C. Platt, and R. Thomale, Phys. Rev. Lett. **110**, 126405 (2013).

[7] W.-S. Wang, Z.-Z. Li, Y.-Y. Xiang, and Q.-H. Wang, Phys. Rev. B **87**, 115135 (2013).

[8] I. I. Mazin, H. O. Jeschke, F. Lechermann, H. Lee, M. Fink, R. Thomale, and R. Valenti, Nat. Commun. **5**, 4261 (2014).

[9] M. Kang, S. Fang, L. Ye, H. C. Po, J. Denlinger, C. Jozwiak, A. Bostwick, E. Rotenberg, E. Kaxiras, J. G. Checkelsky, and R. Comin, Nat. Commun. **11**, 4004 (2020).

[10] M. Kang, L. Ye, S. Fang, J.-S. You, A. Levitan, M. Han, J. I. Facio, C. Jozwiak, A. Bostwick, E. Rotenberg, M. K. Chan, R. D. McDonald, D. Graf, K. Kaznatcheev, E. Vescovo, D. C.

Bell, E. Kaxiras, J. van den Brink, M. Richter, M. P. Ghimire, and J. G. Checkelsky, and R. Comin, Nat. Mater. **19**, 163 (2020).

[11] M. Li, Q. Wang, G. Wang, Z. Yuan, W. Song, R. Lou, Z. Liu, Y. Huang, Z. Liu, H. Lei, Z. Yin, and S. Wang, Nat. Commun. **12**, 3129 (2021).

[12] B. R. Ortiz, L. C. Gomes, J. R. Morey, M. Winiarski, M. Bordelon, J. S. Mangum, I. W. H. Oswald, J. A. Rodriguez-Rivera, J. R. Neilson, S. D. Wilson, E. Ertekin, T. M. McQueen, and E. S. Toberer, Phys. Rev. Mater. **3**, 094407 (2019).

[13] T. Neupert, M. Denner, J. Yin, R. Thomale, and M. Z. Hasan, Nat. Phys. **18**, 137 (2022).

[14] B. R. Ortiz, S. M. L. Teicher, Y. Hu, J. L. Zuo, P. M. Sarte, E. C. Schueller, A. M. M. Abeykoon, M. J. Krogstad, S. Rosenkranz, R. Osborn, R. Seshadri, L. Balents, J. He, and S. D. Wilson, Phys. Rev. Lett. **125**, 247002 (2020).

[15] B. R. Ortiz, P. M. Sarte, E. M. Kenney, M. J. Graf, S. M. L. Teicher, R. Seshadri, and S. D. Wilson, Phys. Rev. Mater. **5**, 034801 (2021).

[16] S.-Y. Yang, Y. Wang, B. R. Ortiz, D. Liu, J. Gayles, E. Derunova, R. Gonzalez-Hernandez, L. Smejkal, Y. Chen, S. S. Parkin, S. D. Wilson, E. S. Toberer, T. Mcqueen, and M. N. Ali, Sci. Adv. **6**, eabb6003 (2020).

[17] H. C. Ku, C. P. Meisner, F. Acker, and D. C. Johnston, Solid State Commun. **35**, 91 (1980).

[18] H. Barz, Mater. Res. Bull. **15**, 1489 (1980).

[19] J. M. Vandenberg and H. Barz, Mater. Res. Bull. **15**, 1493 (1980).

[20] S. K. Malik, A. M. Umarji, G. K. Shenoy, A. T. Aldred, and D. G. Niarchos, Phys. Rev. B **32**, 4742 (1985).

[21] K. S. Athreya, L. S. Hausermann-Berg, R. N. Shelton, S. K. Malik, A. M. Umarji, and G. K. Shenoy, Phys. Lett. A **113**, 330 (1985).

[22] U. Rauchschwalbe, W. Lieke, F. Steglich, C. Godart, L. C. Gupta, and R. D. Parks, Phys. Rev. B **30**, 444(R) (1984).

[23] S. Li, B. Zeng, X. G. Wan, J. Tao, F. Han, H. Yang, Z. H. Wang, and H.-H. Wen, Phys. Rev. B **84**, 214527 (2011).

[24] S. Li, J. Tao, X. G. Wan, X. Ding, and H. Yang, and H.-H. Wen, Phys. Rev. B **86**, 024513 (2012).

[25] B. Li, S. Li, and H.-H. Wen, Phys. Rev. B **94**, 094523 (2016).

[26] C. Mielke, Y. Qin, J.-X. Yin, H. Nakamura, D. Das, K. Guo, R. Khasanov, J. Chang, Z. Q. Wang, S. Jia, S. Nakatsuji, A. Amato, H. Luetkens, G. Xu, M. Z. Hasan, and Z. Guguchia, Phys. Rev. Mater. **5**, 034803 (2021).

[27] C. Gong, S. Tian, Z. Tu, Q. Yin, Y. Fu, R. Luo, and H. Lei, Chin. Phys. Lett. **39**, 087401 (2022).

[28] G. Kresse and J. Hafner, Phys. Rev. B **47**, 558(R) (1993).

[29] G. Kresse and J. Hafner, Phys. Rev. B **49**, 14251 (1994).

[30] G. Kresse and J. Furthmüller, Phys. Rev. B **54**, 11169 (1996).

[31] G. Kresse and J. Furthmüller, Comput. Mater. Sci. **6**, 15 (1996).

[32] G. Kresse and D. Joubert, Phys. Rev. B **59**, 1758 (1999).

[33] J. P. Perdew, K. Burke, and M. Ernzerhof, Phys. Rev. Lett. **77**, 3865 (1996).

[34] P. Giannozzi, O. Baseggio, P. Bonfá, D. Brunato, R. Car, I. Carnimeo, C. Cavazzoni, S. de Gironcoli, P. Delugas, F. F. Ruffino, A. Ferretti, N. Marzari, I. Timrov, A. Urru, and S. Baroni, J. Chem. Phys. **152**, 154105 (2020).

[35] P. Giannozzi, S. Baroni, N. Bonini, M. Calandra, R. Car, C. Cavazzoni, D. Ceresoli, G. L. Chiarotti, M. Cococcioni, I. Dabo, A. D. Corso, S. de Gironcoli, S. Fabris, G. Fratesi, R. Gebauer, U. Gerstmann, C. Gougoussis, A. Kokalj, M. Lazzeri, L. Martin-Samos *et al.*, J. Phys.: Condens. Matter **21**, 395502 (2009).

[36] P Giannozzi, O. Andreussi, T. Brumme, O. Bunau, M. B. Nardelli, M. Calandra, R. Car, C. Cavazzoni, D. Ceresoli, M. Cococcioni, N. Colonna, I. Carnimeo, A. D. Corso, S. de Gironcoli, P. Delugas, R. A. DiStasio, A. Ferretti, A. Floris, G. Fratesi, G. Fugallo, H.-E. Küçükbenli, H.-A. O. de la Roza, S. Poncé *et al.*, J. Phys.: Condens. Matter **29**, 465901 (2017).

[37] D. R. Hamann, Phys. Rev. B **88**, 085117 (2013).

[38] M. Wierzbowska, S. de Gironcoli, and P. Giannozzi, arXiv:cond-mat/0504077.

[39] A. Zeinali, T. Golod, and V. M. Krasnov, Phys. Rev. B **94**, 214506 (2016).

[40] P. Das, C. V. Tomy, S. S. Banerjee, H. Takeya, S. Ramakrishnan, and A. K. Grover, Phys. Rev. B **78**, 214504 (2008).

[41] M. B. Maple, M. C. de Andrade, J. Herrmann, R. P. Dickey, N. R. Dilley, and S. Han, J. Alloys Compd. **250**, 585 (1997).

[42] V. N. Zavaritsky, V. V. Kabanov, and A. S. Alexandrov, Europhys. Lett. **60**, 127 (2002).

[43] Z. X. Shi, M. Tokunaga, T. Tamegai, Y. Takano, K. Togano, H. Kito, and H. Ihara, Phys. Rev. B **68**, 104513 (2003).

[44] Y. Singh, A. Niazi, M. D. Vannette, R. Prozorov, and D. C. Johnston, Phys. Rev. B **76**, 214510 (2007).

[45] Z. Ren, C. Feng, Z. Xu, and M. Fang, and G. Cao, Phys. Rev. B **76**, 132501 (2007).

[46] H. D. Yang, J.-Y. Lin, C. P. Sun, Y. C. Kang, C. L. Huang, K. Takada, T. Sasaki, and H. Sakurai, and E. Takayama-Muromachi, Phys. Rev. B **71**, 020504(R) (2005).

[47] M. Mondal, M. Chand, A. Kamlapure, J. Jesudasan, V. C. Bagwe, S. Kumar, G. Saraswat, V. Tripathi, and P. Raychaudhuri, J. Supercond. Nov. Magn. **24**, 341 (2011).

[48] Y. Singh, C. Martin, S. L. Bud'ko, A. Ellern, R. Prozorov, and D. C. Johnston, Phys. Rev. B **82**, 144532 (2010).

[49] W. L. McMillan, Phys. Rev. **167**, 331 (1968).

[50] J. P. Carbotte, Rev. Mod. Phys. **62**, 1027 (1990).

[51] Y. Zhong, S. Li, H. Liu, Y. Dong, Y. Arai, H. Li, Y. Shi, Z. Wang, S. Shin, H. N. Lee, H. Miao, T. Kondo, and K. Okazaki, arXiv:2207.02407.